Effect of added mass on the interaction of bubbles in a low-Reynolds-number shear flow

Olga Lavrenteva,* Jai Prakash, and Avinoam Nir†
Chemical Engineering Department, TECHNION—Israel Institute of Technology, Haifa 32000, Israel
(Received 4 August 2015; revised manuscript received 7 December 2015; published 8 February 2016)

Equal size air bubbles that are entrapped by a Taylor vortex of the secondary flow in a Couette device, thereby defying buoyancy, slowly form a stable ordered ring with equal separation distances between all neighbors. We present two models of the process dynamics based on force balance on a bubble in the presence of other bubbles positioned on the same streamline in a simple shear flow. The forces taken into account are the viscous resistance, the added mass force, and the inertia-induced repulsing force between two bubbles in a low-Reynolds-number shear flow obtained in Prakash *et al.* [J. Prakash *et al.*, Phys. Rev. E **87**, 043002 (2013)]. The first model of the process assumes that each bubble interacts solely with its nearest neighbors. The second model takes into account pairwise interactions among all the bubbles in the ring. The performed dynamic simulations were compared to the experimental results reported in Prakash *et al.* [J. Prakash *et al.*, Phys. Rev. E **87**, 043002 (2013)] and to the results of quasistationary models (ignoring the added mass effect) suggested in that paper. It is demonstrated that taking into account the effect of added mass, the models describe the major effect of the bubbles' ordering, provide good estimation of the relaxation time, and also predict nonmonotonic behavior of the separation distance between the bubbles, which exhibit over- and undershooting of equilibrium separations. The latter effects were observed in experiments, but are not predicted by the quasistationary models.

DOI: 10.1103/PhysRevE.93.023105

I. INTRODUCTION

In recent years, there has been an ever increasing interest in multiphase flow in Couette-Taylor (CT) devices, which is stimulated by industrial applications such as water purification [1], emulsion polymerization [2,3], liquid-liquid extraction [4], pigment preparation [5], photocatalysis [6], culture of animal cells [7], and cultivation of microalgae [8–12]. Also, bubbly CT flow was used to study the effect of drug reduction caused by bubble injection [13–18]. Experimental and theoretical studies revealed a variety of spatial and spatiotemporal hydrodynamic structures that arise in Couette-Taylor devices [19,20], as well as nontrivial gas bubble spatial distribution [21]. Some recent studies have demonstrated that gas bubbles arrangement may influence the hydrodynamics of the flow considerably. For example, in some cases bubble injection can lead to the increase of the viscous torque in the CT flow [22,23].

Experimental studies of the behavior of individual bubbles embedded in a Couette-Taylor flow at Reynolds numbers corresponding to the first classical instability (Deng *et al.* [24], Byk *et al.* [25]) revealed that equal size bubbles trapped in the vortex core eventually assume an ordered ring with equal separation distances between all neighbors. This phenomenon is attributed to the interaction of bubbles in shear flow. Prakash *et al.* [26] suggested simplified models of multiple bubbles dynamics in the vortex core, assuming small but finite Reynolds number, Re. These models were based on the assumption that the interaction is due mostly to the primary simple shear flow that is considered unbounded in all directions and differs in the assumed mode of interaction, i.e., whether each bubble interacts with its nearest neighbors or with all the bubbles that are present in the device. There exists an inertia-induced force exerted on each bubble in the shear flow, due to the presence of other ones, which is balanced by the Stokes drag. This procedure results in systems of nonlinear ordinary differential equations describing the evolution of the separations between the bubbles. Solutions of these systems were compared to experimental measurements. The Reynolds numbers (at the bubble scale) in the experiments were of the order 1, while the developed theory assumes small values of Re. Nevertheless, the results of computations proved to be in good agreement with the experimental observations; i.e., they describe the main effect of approaching the equilibrium position and provide a good measure of the evolution of relaxation time. However, several interesting phenomena that were observed in several experimental runs at various rotation velocities with two bubbles, such as the overshooting of the equilibrium separation or the reversal of the relative bubble motion and their collision (see [26]), were not reproduced.

Prakash *et al.* [27] studied the case opposite to that considered in [26], i.e., the interaction of bubbles in Couette-Taylor flow at high Reynolds numbers and reported a nonmonotonic behavior of bubbles interaction similar to that observed in several experimental runs reported in [26]. However, this nonmonotonic behavior was found at $\mathrm{Re} \geqslant O(10)$, while in the experiments Re at the bubble scale was of the $O(1)$ and thus, for the nonmonotonic dynamics, only qualitative similarity between theory and experiments was observed. In this paper we demonstrate that taking into account the effect of added mass in the low-Re models may result in nonmonotonic evolution of separation distances at $O(1)$ values of Reynolds number.

II. MODELS OF DYNAMIC INTERACTION OF BUBBLES

Consider a stationary outer cylinder of radius R_{out} and a concentric inner cylinder of radius R_{in} rotating with an angular velocity Ω. The gap between cylinders is filled with a viscous fluid of viscosity η and density ρ. We define the Reynolds

*ceolga@techunix.technion.ac.il
†avinir@techunix.technion.ac.il

number as

$$\mathrm{Re}_{\mathrm{device}} = \Omega\rho R_{\mathrm{in}}(R_{\mathrm{out}} - R_{\mathrm{in}})/\eta.$$

For $\mathrm{Re}_{\mathrm{device}}$ smaller than the critical Reynolds number corresponding to the first instability, the flow is purely azimuthal with the angular velocity

$$u_\theta = \frac{\Omega R_{\mathrm{in}}^2}{R_{\mathrm{out}}^2 - R_{\mathrm{in}}^2}\left(\frac{R_{\mathrm{out}}^2}{r} - r\right). \tag{1}$$

When $\mathrm{Re}_{\mathrm{device}}$ exceeds the critical value, the fluid flow forms counter-rotating cells in the (r, z) plane that are invariant in the azimuthal direction (toroidal vortices). Bubbles introduced in such a flow are trapped either near the wall, at stagnation points, or in the vortex core [24]. We are interested in the interaction and dynamics of these core bubbles.

Consider N spherical bubbles of equal radius a positioned along a center streamline in a Taylor vortex. In the following analysis, length, velocity, time, and stress are rendered nondimensional using a, Ga, $1/G$, and ηG, respectively. Here G is a characteristic shear rate of the primary flow, $G = du_\theta/dr$ at $r = (R_{\mathrm{in}} + R_{\mathrm{out}})/2$. Let $l = \pi(R_{\mathrm{in}} + R_{\mathrm{out}})/a$ be the dimensionless length of this streamline and l_n be the distance between bubbles n and $n+1$. It may be noted that the presence of N bubbles of unit radii implies that $l > 2N$. The distance between bubbles 1 and N can be written as

$$l_N = l - \sum_{n=1}^{N-1} l_n. \tag{2}$$

The values l_n change dynamically due to the repulsive force experienced by bubbles embedded in the shear flow and the drag felt by the bubbles during their translation relative to the flow.

We make the following assumptions in accordance with the assumptions in [26], in order to simplify the analysis:

The interaction is mostly due to the primary shear flow that is considered unbounded in all directions. The effect of the Taylor vortex, that keeps bubbles at a certain horizontal position in the experiment, corresponds to the absence of gravity in the model.

The primary flow is modeled by a unidirectional simple shear, neglecting nonzero curvature of the streamlines. This follows from the diminishingly small ratio of bubble to streamline radii.

The dynamics of translation of bubbles along the streamline connecting their centers results from a balance between the repulsive force induced by the inertia in the shear flow, the viscous resistance to this translation, and the added mass force.

The distances between the bubbles are large compared to their dimensions.

The inertia-induced force on two identical spherical bubbles located along a streamline in a simple shear flow at small Reynolds number, F^{sh}, for the case when the bubbles are within each other's inner viscous region, $d < O(\mathrm{Re}^{-1/2})$, was calculated in [26] as

$$F^{\mathrm{sh}}(d) = \frac{2\pi\,\mathrm{Re}}{9}\left(1 + \frac{1}{d}\right) + O\left(\frac{1}{d^2}\right), \tag{3}$$

where d is the separation between the centers of the bubbles, and the Reynolds number at the bubble scale is $\mathrm{Re} = Ga^2\rho/\eta$. It was shown also in [26] that this force is repulsive (the force exerted on a bubble in a pair is directed away from the second one).

Consider a bubble translating with velocity V, in the presence of M other bubbles located along a line of centers at distances $d_n \gg 1$ from the first one, and translating along the same line with velocities $V_n (n = 1, \ldots, M)$. The Stokes drag on the first bubble is (see, e.g., Happel and Brenner [28])

$$\mathbf{F}^{\mathrm{St}} = -4\pi\left(V - \sum_{n=1}^{M}\frac{V_n}{d_n}\right)\mathbf{e} + O\left(\frac{1}{d^2}\right), \tag{4}$$

with $\mathbf{e}$ denoting a unit vector along the line of centers. The added mass force is

$$\mathbf{F}^{\mathrm{add}} = -\frac{2\pi\,\mathrm{Re}}{3}\frac{dV}{dt}\mathbf{e} + O\left(\frac{1}{d^3}\right). \tag{5}$$

Following [26] we propose further two simplified models of the process that differ in the assumed mode of bubble interaction:

(1) Nearest-neighbors interaction model.
(2) Pairwise interaction model.

Model (1) assumes that each bubble interacts solely with its nearest neighbors on both sides and, thus, results in the following dynamic equations:

$$\begin{aligned}
&\frac{dV_n}{dt} = -\frac{1}{3l_{n-1}} + \frac{1}{3l_n} - \frac{6}{\mathrm{Re}}\left(V_n - \frac{V_{n+1}}{l_n} - \frac{V_{n-1}}{l_{n-1}}\right),\\
&\frac{dl_n}{dt} = V_n - V_{n+1}, \quad n = 1, \ldots, N,\\
&V_{N+1} = V_1, \quad V_0 = V_N, \quad l_0 = l_N.
\end{aligned} \tag{6}$$

Model (2) assumes the pairwise interaction, i.e., that each bubble interacts with each other bubble in the ring as if the others are not present, with the resulting shear-induced force on each bubble being the sum of all forces resulting from these pairwise interactions. The corresponding dynamic system is

$$\begin{aligned}
\frac{dV_n}{dt} &= \frac{1}{3}\sum_{k=1}^{N-1}\left(\frac{1}{l_{n,n+k}} - \frac{1}{l - l_{n,n+k}}\right)\\
&\quad - \frac{6}{\mathrm{Re}}\left[V_n - \sum_{k=1}^{N-1}\left(\frac{V_{n+k}}{|l_{n,n+k}|} + \frac{V_{n-k}}{|l_{n,n-k}|}\right)\right],\\
\frac{dl_n}{dt} &= V_n - V_{n+1}, \quad n = 1, \ldots, N,
\end{aligned} \tag{7}$$

where

$$\begin{aligned}
&l_{n,k} = \sum_{j=n\lessgtr k}^{k} l_j, \quad \sum_{j=k}^{n} l_j = -\sum_{j=n}^{k} l_j, \quad n,k = 1, \ldots, N,\\
&V_{N+k} = V_k, \quad V_{-k} = V_{N-k}, \quad V_0 = V_N,\\
&l_{N+k} = l_k, \quad l_{-k} = l_{N-k}, \quad l_0 = l_N.
\end{aligned}$$

It follows from the equations above, that $\sum_{n=1}^{N} l_n = l$ is an integral of these systems. In cases of two and three bubbles considered below, (2) will be used to reduce the order of the system by 1. Also, one can see that both systems (6) and (7) have stationary solutions $l_n = l/N$, $V_n = 0$, $n = 1, \ldots, N$. Following [27], we first linearize the equations in the vicinity

of these stationary solutions and study the obtained linear systems. The nonlinear effects are then studied via numerical simulations of systems (6) and (7).

III. RESULTS

A. Linearized equations

Linearization of (6) in the vicinity of the stationary solution results in

$$\begin{aligned}\frac{dV_n}{dt} &= \frac{N^2}{3l^2}(\xi_{n-1}-\xi_n) \\ &\quad -\frac{6}{\mathrm{Re}}\left(V_n-\frac{NV_{n+1}}{l}-\frac{NV_{n-1}}{l}\right), \\ \frac{d\xi_n}{dt} &= V_n - V_{n+1}, \quad n=1,\ldots,N, \\ V_{N+1} &= V_1, \quad V_0 = V_N, \quad \xi_0 = \xi_N, \end{aligned} \tag{8}$$

where $l_n = l/N + \xi_n$, ξ_n, $V_n = 1$, $n = 1,\ldots,N$.

Similarly, linearization of (7) leads to

$$\begin{aligned}\frac{dV_n}{dt} &= \frac{N^2}{3l^2}\sum_{k=1}^{N}\frac{1}{k^2}\left(\sum_{j=n-k}^{n-1}\xi_j - \sum_{j=n}^{n+k-1}\xi_j\right) \\ &\quad -\frac{6}{\mathrm{Re}}\left(V_n-\frac{N}{l}\sum_{k=1}^{N-1}\frac{V_{n+k}+V_{n-k}}{k}\right), \\ \frac{d\xi_n}{dt} &= V_n - V_{n+1}, \quad n=1,\ldots,N, \\ \xi_{N+k} &= \xi_k, \quad \xi_{-k} = \xi_{N-k}, \quad \xi_0 = \xi_N. \end{aligned} \tag{9}$$

Both systems are of the order $2N$. However, it is easy to see that

$$V(t) = \sum_{n=1}^{N} V_n(t) = V(0)\exp\left[-\frac{6}{\mathrm{Re}}\left(1-\frac{2N}{l}\right)t\right]$$

for solutions of (8), while for solution of (9),

$$V(t) = \sum_{n=1}^{N} V_n(t) = V(0)\exp\left[-\frac{6}{\mathrm{Re}}\left(1-\frac{2N}{l}\sum_{k=1}^{N-1}\frac{1}{k}\right)t\right].$$

Also, $\sum_{n=1}^{N}\xi_n = \mathrm{const} = 0$ for both systems. Thus, their order can be reduced by 2. Introduction of new variables, $U_n = V_{n+1} - V_n$, $n = 1,\ldots,N-1$, simplifies the systems (8) and (9) to the forms

$$\begin{aligned}\frac{dU_n}{dt} &= \frac{N^2}{3l^2}(\xi_{n-1}-2\xi_n+\xi_{n+1}) \\ &\quad -\frac{6}{\mathrm{Re}}\left(U_n-\frac{NU_{n+1}}{l}-\frac{NU_{n-1}}{l}\right), \\ \frac{d\xi_n}{dt} &= U_n, \quad n=1,K,N-1, \\ U_N &= U_0 = -\sum_{n=1}^{N-1}U_n, \quad \xi_0 = \xi_N = -\sum_{n=1}^{N-1}\xi_n, \end{aligned} \tag{10}$$

and

$$\begin{aligned}\frac{dU_n}{dt} &= \frac{N^2}{3l^2}\sum_{k=1}^{N-1}\frac{\xi_{n-k}-2\xi_n+\xi_{n+k}}{k^2} \\ &\quad -\frac{6}{\mathrm{Re}}\left(U_n-\frac{N}{l}\sum_{k=1}^{N-1}\frac{U_{n-k}+U_{n+k}}{k}\right), \\ \frac{d\xi_n}{dt} &= U_n, \quad n=1,K,N-1, \quad U_{N+k}=U_k, \\ U_{-k} &= U_{N-k}, \quad U_N = U_0 = -\sum_{n=1}^{N-1}U_n, \\ \xi_{N+k} &= \xi_k, \quad \xi_{-k} = \xi_{N-k}, \quad \xi_0 = \xi_N = -\sum_{n=1}^{N-1}\xi_n, \end{aligned} \tag{11}$$

respectively.

When only two bubbles are trapped by the vortex, the two models coincide and result in the following dynamic equations:

$$\frac{d\xi_1}{dt} = U_1, \quad \frac{dU_1}{dt} = -\frac{16}{3l^2}\xi_1 - \frac{6}{\mathrm{Re}}\left(1+\frac{4}{l}\right)U_1\ . \tag{12}$$

The general solution of (12) is

$$\begin{aligned}\xi_1 &= c_1\exp(\lambda_1 t) + c_2\exp(\lambda_2 t), \\ U_1 &= c_1\lambda_1\exp(\lambda_1 t) + c_2\lambda_2\exp(\lambda_2 t), \\ \lambda_{1,2} &= -\frac{3}{\mathrm{Re}}\left(1+\frac{4}{l}\right)\left[1\pm\sqrt{1-\frac{16\mathrm{Re}^2}{27(l+4)^2}}\right]. \end{aligned} \tag{13}$$

In the last expression, indices 1 and 2 correspond to signs "–" and "+," respectively.

It follows from (13) that there exists a critical Reynolds number, $\mathrm{Re}^{\mathrm{cr}} = 3\sqrt{3}(1+l/4)$. If $\mathrm{Re} > \mathrm{Re}^{\mathrm{cr}}$, the eigenvalues are complex and the solution exhibits an oscillatory behavior with exponentially decaying amplitude, while for subcritical Reynolds number, $\mathrm{Re} < \mathrm{Re}^{\mathrm{cr}}$, the eigenvalues are real and, at asymptotically large time, relative distances between the bubbles change monotonically.

We define the relaxation time T_{rel} to be the time in which the deviations from equilibrium decrease tenfold. In the framework of the linear theory, the relaxation time is determined by an eigenvalue $\lambda = \lambda_{\mathrm{re}} + i\lambda_{\mathrm{im}}$ having real part with minimal absolute value (i.e., corresponding to the slowest decaying disturbances), $T_{\mathrm{rel}} = 3/|\lambda_{\mathrm{re}}|$. In the case of two bubbles, obviously, $\lambda = \lambda_1$. The dependence of the relaxation time on the Reynolds number for various l is illustrated in Fig. 1. We chose the values of l corresponding to the experiments with two ($l = 263.4$) and more ($l = 209$) bubbles reported in [26]. $l = 100$ was used in our previous paper [27], where the case of large Re was studied.

It is evident in Fig. 1 that $T_{\mathrm{rel}}(\mathrm{Re})$ decays fast at subcritical Re. It reaches a minimum at $\mathrm{Re} = \mathrm{Re}^{\mathrm{cr}}$, and slowly grows at supercritical Re. Also, as can be expected, the relaxation time increases with the length of the closed streamline l. Qualitatively, similar behavior was found for the high-Re asymptotic model (see [27], Fig. 7), but for that case, the linear theory predicts much higher values of the critical Re of $O(10^4)$.

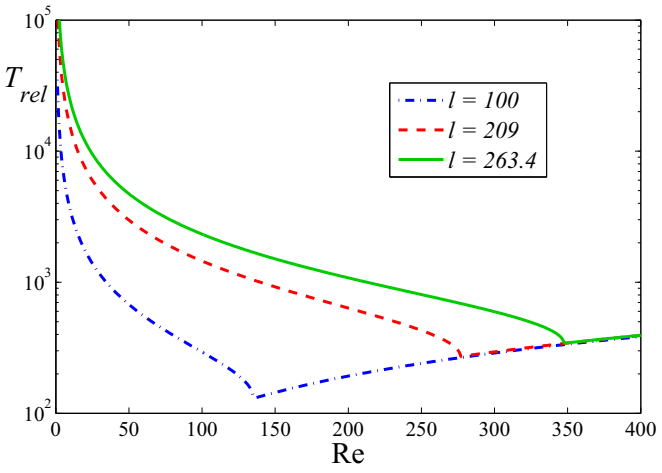

FIG. 1. Relaxation time in the case of two bubbles.

Note that in the experimental devices, $l \geqslant O(10^2)$ and $\mathrm{Re} \leqslant O(10)$, see, e.g., [26], while $\mathrm{Re}^{\mathrm{cr}} = 3\sqrt{3}(1 + l/4) \geqslant O(10^2)$. Thus, as far as these experimental results are concerned, subcritical Reynolds numbers are of interest. The constants c_1 and c_2 in (13) are determined from the initial conditions

$$\xi(0) = \xi_0, \quad U(0) = U_0. \tag{14}$$

It is easy to show that, in the framework of the linear theory, if $\lambda_2 \leqslant U_0/\xi_0 \leqslant 0$, the initially shorter (longer) separation between the bubbles monotonically increases (decreases) and tends to its equilibrium value $l/2$. In the case $U_0/\xi_0 > 0$, the initially shorter (longer) separation first decreases (increases), reaches a minimum (maximum) and then approaches the equilibrium value. Finally, if the initial conditions satisfy $U_0/\xi_0 < \lambda_2 < 0$, the initially shorter (longer) separation exhibits over- (under-) shooting of the equilibrium value. The latter effect was observed in experiments reported in [24–26] but was not predicted by the models suggested there. The experimental run with an overshooting, demonstrated in Fig. 12 of [26], corresponds to $l = 263.4$ and $\mathrm{Re} = 0.7$, which leads to $\lambda_1 = -1.31 \times 10^{-5}$, $\lambda_2 = -8.74$. Following [27] we define a relaxation time as $T_{\mathrm{rel}} = 3/|\lambda_1| \simeq 2.29 \times 10^5$ corresponding to the dimensional time of 57 *min*, that agrees with the experimental observation. On the other hand, if the initial relative velocity is negative, the bubbles first approach each other and, if the initial separation is small, they may collide. This effect was also observed in several experimental runs and no explanation was found in the framework of the model suggested in [26].

In the case of three bubbles, the two models lead to different ordinary differential equation (ODE) systems. Namely, the nearest-neighbor interaction model results in

$$\begin{aligned} \frac{dU_i^{(1)}}{dt} &= -\frac{9\xi_i^{(1)}}{l^2} - \frac{6}{\mathrm{Re}}\left(1 + \frac{3}{l}\right)U_i^{(1)}, \\ \frac{d\xi_i^{(1)}}{dt} &= U_i^{(1)}, \quad i = 1,2, \end{aligned} \tag{15}$$

and the pairwise interaction model leads to

$$\begin{aligned} \frac{dU_i^{(2)}}{dt} &= -\frac{45}{4}\frac{\xi_i^{(2)}}{l^2} - \frac{6}{\mathrm{Re}}\left(1 + \frac{9}{2l}\right)U_i^{(2)}, \\ \frac{d\xi_i^{(2)}}{dt} &= U_i^{(2)}, \quad i = 1,2. \end{aligned} \tag{16}$$

Here and below, upper indices (1) and (2) correspond to the nearest neighbors and pairwise interaction models, respectively.

The general solutions of these equations are

$$\begin{aligned} U_1^{(j)} &= c_1^{(j)}\lambda_1^{(j)}\exp\left(\lambda_1^{(j)}t\right) + c_2^{(j)}\lambda_2^{(j)}\exp\left(\lambda_2^{(j)}t\right), \\ \xi_1^{(j)} &= c_1^{(j)}\exp\left(\lambda_1^{(j)}t\right) + c_2^{(j)}\exp\left(\lambda_2^{(j)}t\right), \\ U_2^{(j)} &= c_3^{(j)}\lambda_2^{(j)}\exp\left(\lambda_2^{(j)}t\right) + c_4^{(j)}\lambda_2^{(j)}\exp\left(\lambda_2^{(j)}t\right), \\ \xi_2^{(j)} &= c_3^{(j)}\exp\left(\lambda_2^{(j)}t\right) + c_4^{(j)}\exp\left(\lambda_2^{(j)}t\right), \quad j = 1, 2, \end{aligned} \tag{17}$$

$$\lambda_{1,2}^{(1)} = -\frac{3}{\mathrm{Re}}\left(1 + \frac{3}{l}\right)\left[1 \pm \sqrt{1 - \frac{\mathrm{Re}^2}{(l+3)^2}}\right],$$

$$\lambda_{1,2}^{(2)} = -\frac{3}{\mathrm{Re}}\left(1 + \frac{9}{2l}\right)\left[1 \pm \sqrt{1 - \frac{5\mathrm{Re}^2}{(2l+9)^2}}\right].$$

One can see that both models predict critical Reynolds numbers, beyond which eigenvalues are complex and the solution oscillates at large time: $\mathrm{Re}^{\mathrm{cr},(1)} = l + 3$ and $\mathrm{Re}^{\mathrm{cr},(2)} = (2l + 9)/\sqrt{5}$. Both values are smaller than the critical Re for the two-bubble configuration and $\mathrm{Re}^{\mathrm{cr},(2)} < \mathrm{Re}^{\mathrm{cr},(1)}$ for $l > 10$.

In Fig. 2, the relaxation time of the three-bubble system calculated according to models (1) and (2) is plotted versus the Reynolds number for $l = 209$ (as in [26]) and $l = 100$ (as in [27]). It is evident that the pairwise interaction model predicts faster relaxation than the nearest-neighbors one and that T_{rel} increases with increase of the length l.

In the case of four bubbles the eigenvalues of systems (10) and (11) are

$$\begin{aligned} \lambda_{1,2}^{(1)} &= -\frac{3}{\mathrm{Re}}\left[1 \pm \sqrt{1 - \frac{32}{27l^2}\mathrm{Re}^2}\right], \\ \lambda_{3,4}^{(1)} &= -\frac{3}{\mathrm{Re}}\left(1 + \frac{8}{l}\right)\left[1 \pm \sqrt{1 - \frac{64\mathrm{Re}^2}{27(l+8)^2}}\right], \end{aligned} \tag{18}$$

and

$$\begin{aligned} \lambda_{1,2}^{(2)} &= -\frac{3}{\mathrm{Re}}\left(1 + \frac{4}{l}\right)\left[1 \pm \sqrt{1 - \frac{16 \times 29\mathrm{Re}^2}{243(l+4)^2}}\right], \\ \lambda_{3,4}^{(2)} &= -\frac{1}{\mathrm{Re}}\left(3 + \frac{20}{l}\right)\left[1 \pm \sqrt{1 - \frac{640\mathrm{Re}^2}{27(3l+20)^2}}\right], \end{aligned} \tag{19}$$

respectively. In Eqs. (18) and (19), the lower indices 1 and 3 correspond to "+" on the right-hand side, while 2 and 4 correspond to "–." Again, as in systems with two and three bubbles, oscillations take place beyond some critical Reynolds number with $\mathrm{Re}^{\mathrm{cr},(1)} = 3\sqrt{3}(l/8 + 1)/8 \simeq 0.65(l + 8)$, for the nearest-neighbors model, and $\mathrm{Re}^{\mathrm{cr},(2)} = 3\sqrt{30}(3l + 20)/80 \simeq$

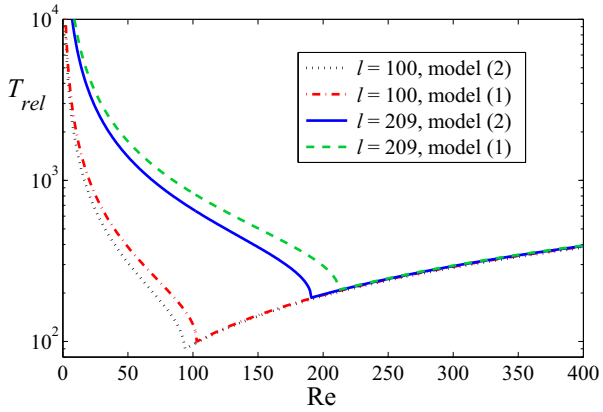

FIG. 2. Relaxation time in the case of three bubbles.

$0.62(l+7)$ for the pairwise interaction one. Both values are smaller than the critical Re for the three-bubble configuration and $\mathrm{Re}^{\mathrm{cr},(2)} < \mathrm{Re}^{\mathrm{cr},(1)}$ for $l > 60$.

In Fig. 3, the relaxation time of a four-bubble system, calculated according to models (1) and (2), is plotted versus the Reynolds number for $l = 209$ (as in [26]) and $l = 100$ (as in [27]). One can see that the pairwise interaction model predicts faster relaxation than the nearest-neighbors-interaction one, and that T_{rel} increases with the increase of the length l. For conditions corresponding to the experiments with three and four bubbles described in [26], $l = 209$ and $\mathrm{Re} = 1.23$ correspond to subcritical values of the Reynolds numbers. In this case, all the eigenvalues are real and negative, and the relaxation time is close to the one obtained by the model ignoring added mass effect used in [26]. However, as in the case of two bubbles, the model of the present paper predicts over- (under-) shooting of the initially minimal (maximal) separation distance between the bubbles as well as bubble collisions for certain initial conditions, effects that were observed experimentally and were not explained by the model of [26].

Studying linearized systems with more than four bubbles reveals a complicated behavior with multiple modes of oscillations and damping. However, several qualitative features and trends remain similar: The solutions either exhibit collision

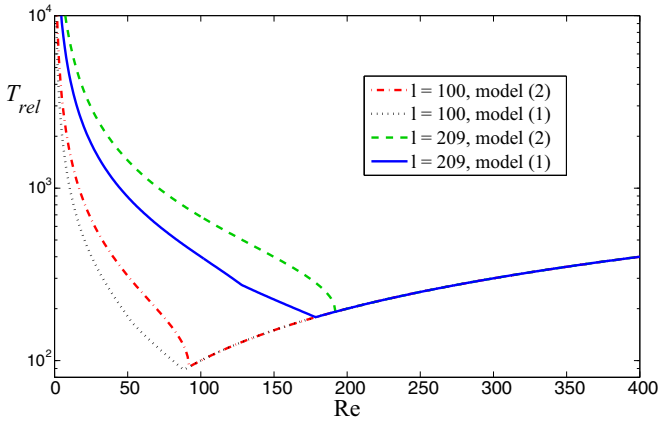

FIG. 3. Relaxation time in the case of four bubbles.

of two bubbles or tend to equilibrium. In the latter case, there is a critical Reynolds number above which oscillations are observed. The critical Re grows linearly with l and slowly decreases with the number of bubbles N. The two models of bubbles interaction predict close values of critical Re, with the one obtained by the nearest-neighbors model being a little lower at high enough values of l. Over- (under-) shooting of the initially minimal (maximal) separation distance between the bubbles is observed for certain initial conditions both in sub- and supercritical regimes.

B. Numerical solutions of the nonlinear equations

The nonlinear effects were studied via numerical integration of the systems (10) and (11). When only two bubbles are trapped by the vortex, the two models coincide and result in the following dynamic equations:

$$\begin{aligned}
\frac{dV_1}{dt} &= -\frac{1}{3(l-l_1)} + \frac{1}{3l_1} - \frac{6}{\mathrm{Re}}\left(V_1 - \frac{V_2}{l-l_1} - \frac{V_2}{l_1}\right),\\
\frac{dV_2}{dt} &= -\frac{1}{3l_1} + \frac{1}{3(l-l_1)} - \frac{6}{\mathrm{Re}}\left(V_2 - \frac{V_1}{l-l_1} - \frac{V_1}{l_1}\right)\\
\frac{dl_1}{dt} &= V_1 - V_2.
\end{aligned} \tag{20}$$

Introduction of new variables $U = V_1 - V_2$, $V = V_1 + V_2$ simplifies Eq. (20) to

$$\begin{aligned}
\frac{dU}{dt} &= -\frac{2}{3l_1} + \frac{2}{3(l-l_1)} - \frac{6U}{\mathrm{Re}}\left(1 + \frac{1}{l-l_1} + \frac{1}{l_1}\right),\\
\frac{dl_1}{dt} &= U,
\end{aligned} \tag{21}$$

$$\frac{dV}{dt} = -\frac{6V}{\mathrm{Re}}\left(1 - \frac{1}{l-l_1} - \frac{1}{l_1}\right). \tag{22}$$

It is evident that the system (21) can be solved independently of (22), providing the evolution of the separation between two bubbles l_1 and the relative velocity U. As soon as $l_1(t)$ is determined, the variable V can be found by integrating (22) to give

$$V(t) = V(0)\exp\left\{-\frac{6}{\mathrm{Re}}\int_0^t \left[1 - \frac{1}{l-l_1(\tau)} - \frac{1}{l_1(\tau)}\right]d\tau\right\}. \tag{23}$$

The performed calculations demonstrated that, as anticipated and predicted by the linear analysis, either a pair of neighboring bubbles collide, or, with the passage of time, the system assumes an equilibrium configuration with equal separations between the neighbors. In the latter case 3 different regimes of system evolution are possible: Monotonic growth of the initially minimal separation distance, overshooting of equilibrium, and oscillations. Examples of such a behavior are presented in Fig. 4, where the evolution of the initially minimal separation distance is depicted for several initial conditions and Reynolds numbers. In Fig. 4(a), the bubbles are initially separated by ten radii and have equal velocity. The repulsive force induces relative motion of the bubbles and the separation distance increases. The presence of viscous force causes a damping effect and, with the passage of time,

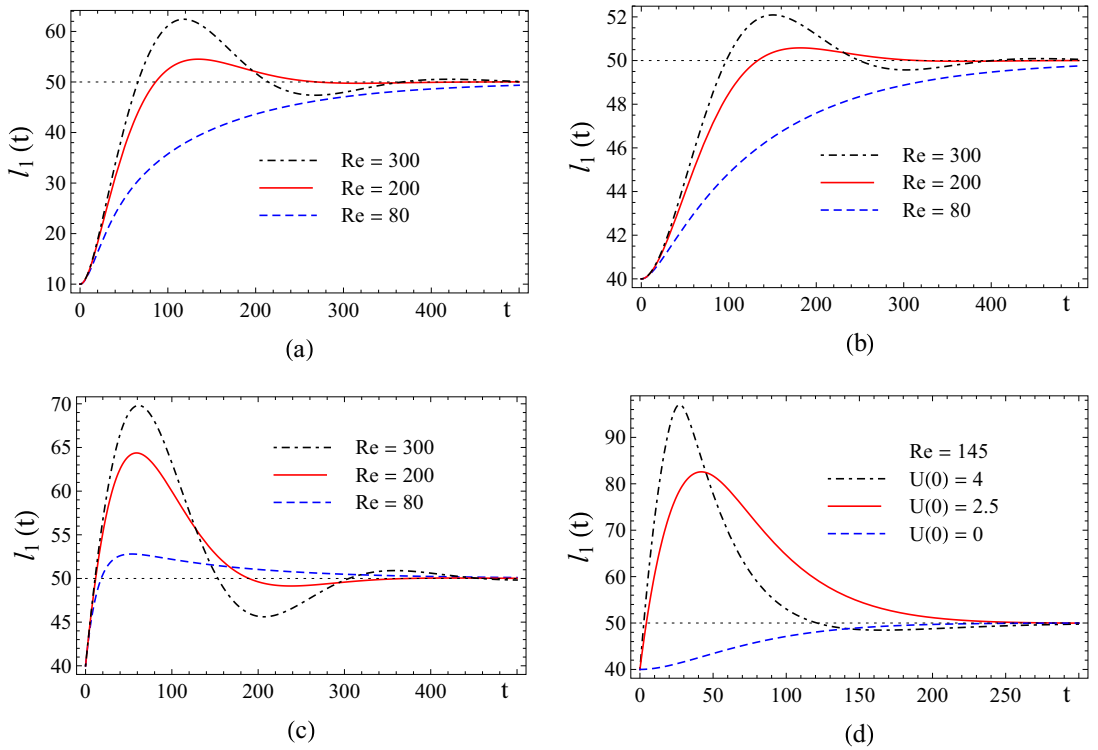

FIG. 4. Evolution of the initially minimal separation distance between two bubbles scaled by bubbles radius. Time t is scaled by $1/G$. (a) $l_1(0) = 10$, $U(0) = 0$; (b) $l_1(0) = 40$, $U(0) = 0$; (c) $l_1(0) = 40$, $U(0) = 1$; (d) $l_1(0) = 40$, Re $= 145$. Equilibrium separation is shown by dotted line.

the relative velocity of the bubbles decays and the bubbles assume an equilibrium position. For relatively low Re, the separation distance increases monotonically and approaches the equilibrium value from below, while for higher Re, overshooting of the equilibrium separation and oscillatory behavior are observed. In Fig. 4(b), the bubbles are initially separated by 40 radii and move with equal velocity. For each value of Re, the behavior of the bubbles is qualitatively the same as in the lower initial separation case, with somewhat smaller overshooting and smaller amplitude of oscillations. In Fig. 4(c), the bubbles are initially separated by 40 radii and have a scaled relative velocity of 1. In this case, the interaction patterns change considerably compared to the case of equal initial velocities. For high Re $= 300$, the amplitude of oscillations increases and the period decreases. For Re $= 200$, oscillations are evident for $U(0) = 1$, while for $U(0) = 0$, the separation distance exhibits a single maximum. For lower value of Re $= 80$, the separation distance grows monotonically when $U(0) = 0$, and it exhibits a single maximum if $U(0) = 1$. Figure 4(d) demonstrates that all three evolution scenarios are possible for the same value of Re and initial separation if the initial relative velocity is changed.

For high enough initial relative velocity, the bubbles will collide. Analysis of the computation results leads to the conclusion that the scenario of the interaction is determined by the Reynolds number and by the initial relative velocity of the bubbles, while the initial separation affects solely the amplitude of oscillations and the heights of overshooting. This is valid also if a larger number of bubbles exists in the system. In what follows, we focus on the effect of Re and initial velocity on the evolution of separations between the bubbles.

In the case of more than two bubbles, the two models lead to different ODE systems. For example, in the three bubbles case the nearest-neighbor interaction models results in

$$\begin{aligned}
\frac{dV_1}{dt} &= -\frac{1}{3(l-l_1-l_2)} + \frac{1}{3l_1} \\
&\quad - \frac{6}{\mathrm{Re}}\left(V_1 - \frac{V_2}{l_1} - \frac{V_3}{l-l_1-l_2}\right), \\
\frac{dV_2}{dt} &= -\frac{1}{3l_1} + \frac{1}{3l_2} - \frac{6}{\mathrm{Re}}\left(V_2 - \frac{V_3}{l_2} - \frac{V_1}{l_1}\right), \\
\frac{dV_3}{dt} &= -\frac{1}{3l_2} + \frac{1}{3(l-l_1-l_2)} \\
&\quad - \frac{6}{\mathrm{Re}}\left(V_3 - \frac{V_1}{(l-l_1-l_2)} - \frac{V_2}{l_2}\right), \\
\frac{dl_1}{dt} &= V_1 - V_2, \quad \frac{dl_2}{dt} = V_2 - V_3.
\end{aligned} \tag{24}$$

Results of the numerical solution of (24) with $l = 100$, $l_1(0) = 15$, $l_2(0) = 25$, and various Re and initial velocities are presented in Fig. 5, where the separation distances l_1, l_2, and $l_3 = l - l_1 - l_2$ are plotted versus scaled time. The left and right columns in Fig. 5 are computed with Re $= 200$ and 80, respectively. In Figs. 5(a) and 5(b) all the initial velocities equal zero. One can see that at lower Reynolds number, all the separations monotonically approach the equilibrium value of $l/3$, while for higher Re, oscillatory behavior is evident. In Figs. 5(c) and 5(d), bubbles 2 and 3 are initially stationary, while bubble 1 moves. As a result, the separation $l_1(l_3)$ increases (decreases) faster than in the previous case of zero initial velocities, and exhibits an over- (under-) shooting

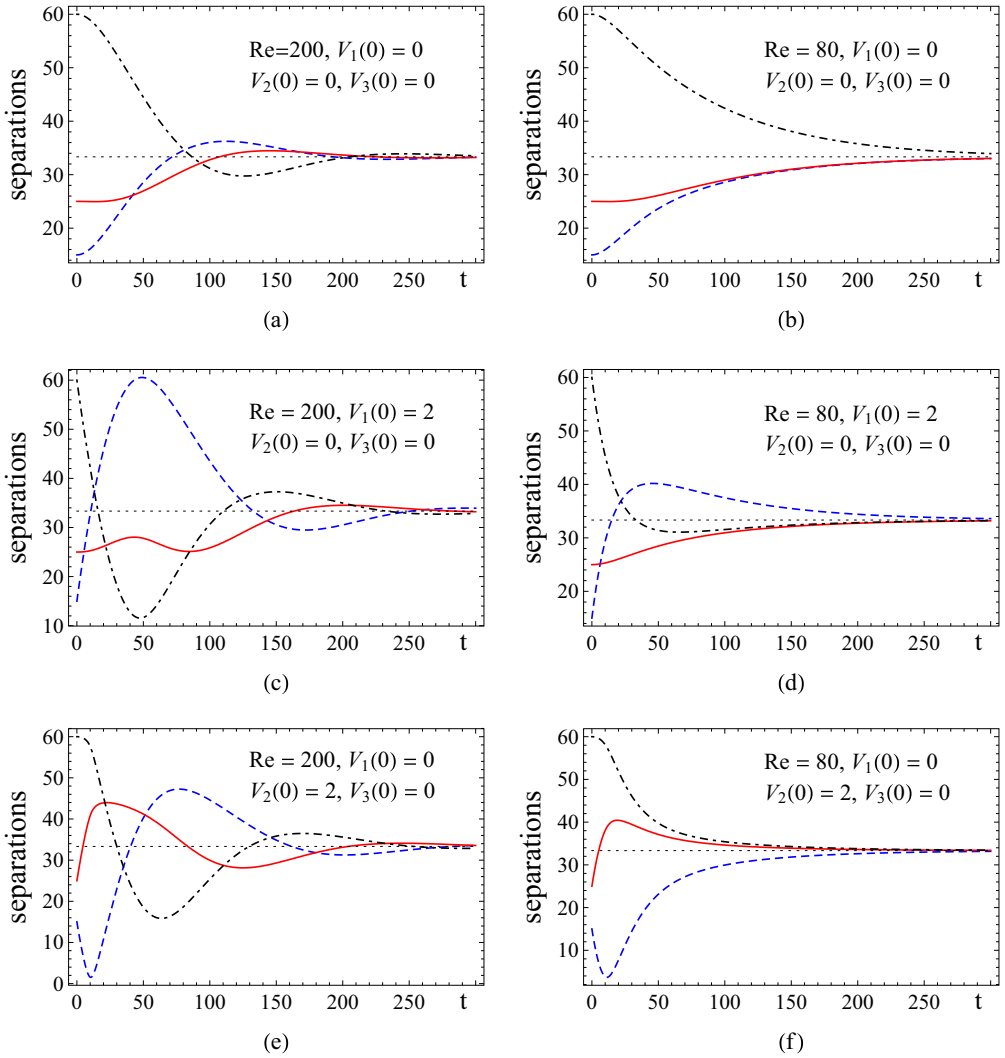

FIG. 5. Evolution of separation distances in the case of three bubbles for $l = 100$, $l_1(0) = 15$, $l_2(0) = 25$, and various Reynolds numbers and initial velocities. Separations are scaled by bubbles radius. Time t is scaled by $1/G$. Nearest-neighbors interaction model. $l_1(t)$, $l_2(t)$, and $l_3(t)$ are shown by dashed, solid, and dashed-dotted curves, respectively.

of the equilibrium values even for low Re. For higher values of Re, the amplitude of oscillations is higher and the period is shorter. The repulsive force induces a relative motion of the bubbles and the separation distance increases.

In Figs. 5(e) and 5(f), bubbles 1 and 3 are initially stationary, while bubble 2 moves. As a result, the initially shortest separation l_1 decreases, achieves a minimum, and then increases. The separation l_2 grows faster than in the previous cases and exhibits overshooting of the equilibrium value. In this case, again, one can see oscillations at high Re, and monotonic approach to equilibrium for lower Re at relatively large t. The pairwise interaction model in the case of three bubbles leads to

$$\frac{dV_1}{dt} = -\frac{1}{3(l-l_1-l_2)} + \frac{1}{3l_1} - \frac{1}{3(l-l_1)} + \frac{1}{3(l_1+l_2)} - \frac{6}{\mathrm{Re}}\left[V_1 - V_2\left(\frac{1}{l_1} + \frac{1}{l-l_1}\right) - V_3\left(\frac{1}{l_1+l_2} + \frac{1}{l-l_1-l_2}\right)\right],$$

$$\frac{dV_2}{dt} = -\frac{1}{3l_1} + \frac{1}{3(l-l_1)} - \frac{1}{3(l-l_2)} + \frac{1}{3l_2} - \frac{6}{\mathrm{Re}}\left[V_2 - V_3\left(\frac{1}{l_2} + \frac{1}{l-l_2}\right) - V_1\left(\frac{1}{l_1} + \frac{1}{l-l_1}\right)\right],$$

$$\frac{dV_3}{dt} = -\frac{1}{3l_2} + \frac{1}{3(l-l_2)} - \frac{1}{3(l_1+l_2)} + \frac{1}{3(l-l_1-l_2)} - \frac{6}{\mathrm{Re}}\left[V_3 - V_1\left(\frac{1}{l_1+l_2} + \frac{1}{l-l_1-l_2}\right) - V_2\left(\frac{1}{l_2} + \frac{1}{l-l_2}\right)\right],$$

$$\frac{dl_1}{dt} = V_1 - V_2, \quad \frac{dl_2}{dt} = V_2 - V_3. \tag{25}$$

An example of numerical solution of (25) and a comparison with the solution of (24) with $l = 100$, $l_1(0) = 15$, $l_2(0) = 25$, $U_1(0) = 1$, $U_2(0) = U_3(0) = 0$ are presented in Fig. 6. In Figs. 6(a) and 6(c) Re = 200, while in Figs. 6(b) and 6(d) Re = 80. In Figs. 6(a) and 6(b), the separation distances l_1, l_2,

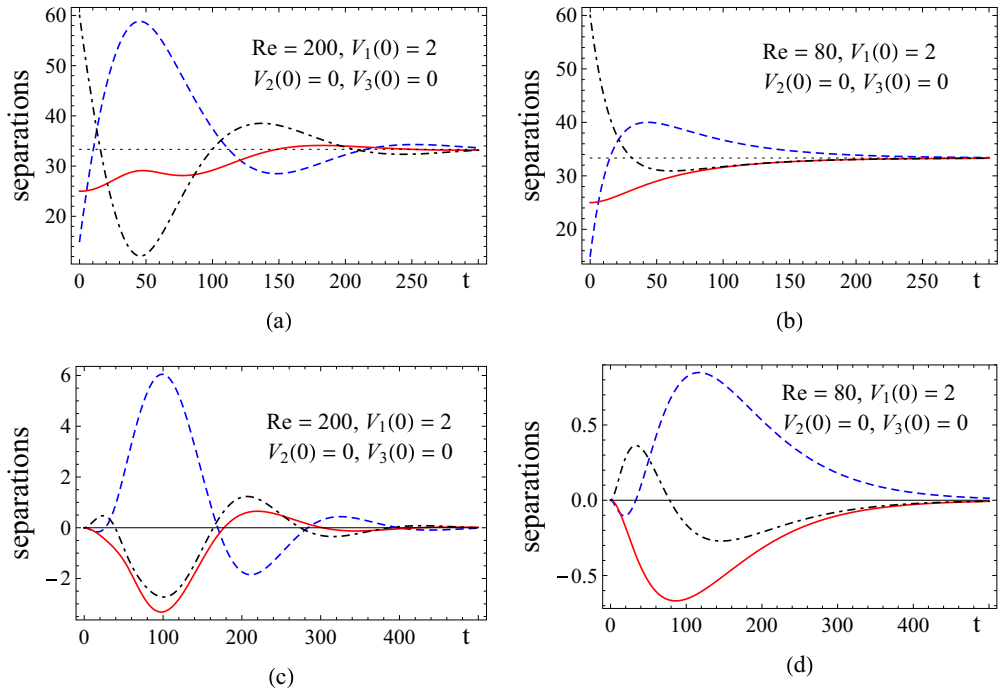

FIG. 6. Separation distances in the case of three bubbles for $l = 100$, $l_1(0) = 15$, $l_2(0) = 25$, and various Reynolds numbers and initial velocities. $l_1(t)$, $l_2(t)$, and $l_3(t)$ are shown by dashed, solid, and dashed-dotted curves, respectively. (a,b) present the evolution of separation distances computed with pairwise interaction model (25). (c,d) show the differences of separation distances computed with Eqs. (24) and (25).

and $l_3 = l - l_1 - l_2$ are plotted versus time. In Figs 6(c) and 6(d), the differences of separation distances computed with Eqs. (24) and (25) are presented. One can see that the results of the two models depicted in Figs. 5 and 6 give similar interaction patterns, with somewhat smaller amplitude of oscillations and faster damping observed in model (2).

On the right-hand column of Figs. 5 and 6 one can observe that two separation distances become very close well before they approach equilibrium values. Thus, it can be anticipated that systems (24) and (25) obtain solutions with two equal separations, say $l_1 = l_2$, that serve as intermediate asymptotics for some classes of solutions. Indeed, if $l_1(0) = l_2(0)$ and $U_2(0) = 0$, $U_1(0) + U_3(0) = 0$, the analogous equalities are valid at any moment of time and systems (24) and (25) can be simplified to

$$\begin{aligned} \frac{dU_1}{dt} &= \frac{1}{3l_1} - \frac{1}{3(l-2l_1)} - \frac{6U_1}{\mathrm{Re}}\left(1 + \frac{1}{l-2l_1}\right), \\ \frac{dl_1}{dt} &= U_1, \end{aligned} \tag{26}$$

and

$$\begin{aligned} \frac{dU_1}{dt} &= \frac{1}{2l_1} - \frac{1}{3(l-2l_1)} - \frac{1}{3(l-l_1)} \\ &\quad - \frac{6U_1}{\mathrm{Re}}\left(1 + \frac{1}{2l_1} + \frac{1}{l-2l_1}\right), \\ \frac{dl_1}{dt} &= U_1, \end{aligned} \tag{27}$$

respectively.

Numerical simulations of systems with more than three bubbles reveal several qualitative features and trends of the process that take place for $N = 2$ and 3 as well: The solutions either exhibit collision of two bubbles or tend to equilibrium. In the latter case, there is a critical Reynolds number, above which the oscillations are an observed behavior. The critical Re grows with l and slowly decreases with the number of bubbles N. In contrast to the linearized model, this critical Re depends also on the initial relative velocities of the bubbles. The latter effect was observed in [27] for the low-viscosity models of interaction, where it was found that the critical Reynolds number drastically decreases with the growth of the initial velocity of the bubbles relative to that of the ambient fluid, from $O(10^5)$ for the bubbles initially moving with the flow to $O(10^2)$ for the case when quiescent bubbles are introduced into a moving fluid, and the initial relative velocity equals that of the fluid at the center streamline in the Couette-Taylor device described in [24–26]. In contrast to this, for high-viscosity models considered in the present paper, the critical value of Re remains of the same order of magnitude of $O(10 - 10^2)$ for all the initial conditions.

Note that in the experiments reported in [24–26], the Reynolds numbers at the bubble scale are of the order 1. Thus, subcritical regimes, where no oscillations are anticipated, are of interest. However, taking into account the effect of added mass results in a prediction of over- (under-) shooting of the equilibrium values for the initially minimal (maximal) separation also in the subcritical regime, if the parameters l, Re, $l_1(0)$, $U_1(0)$ are located in a certain subdomain of physically relevant parameters $\{l, \mathrm{Re}, 2 < l_1(0) < l/2, 0 < U_1(0) < 10\}$ in $\mathbf{R}^4$ space. $l_1(0) > 2$ means that the bubbles' boundaries

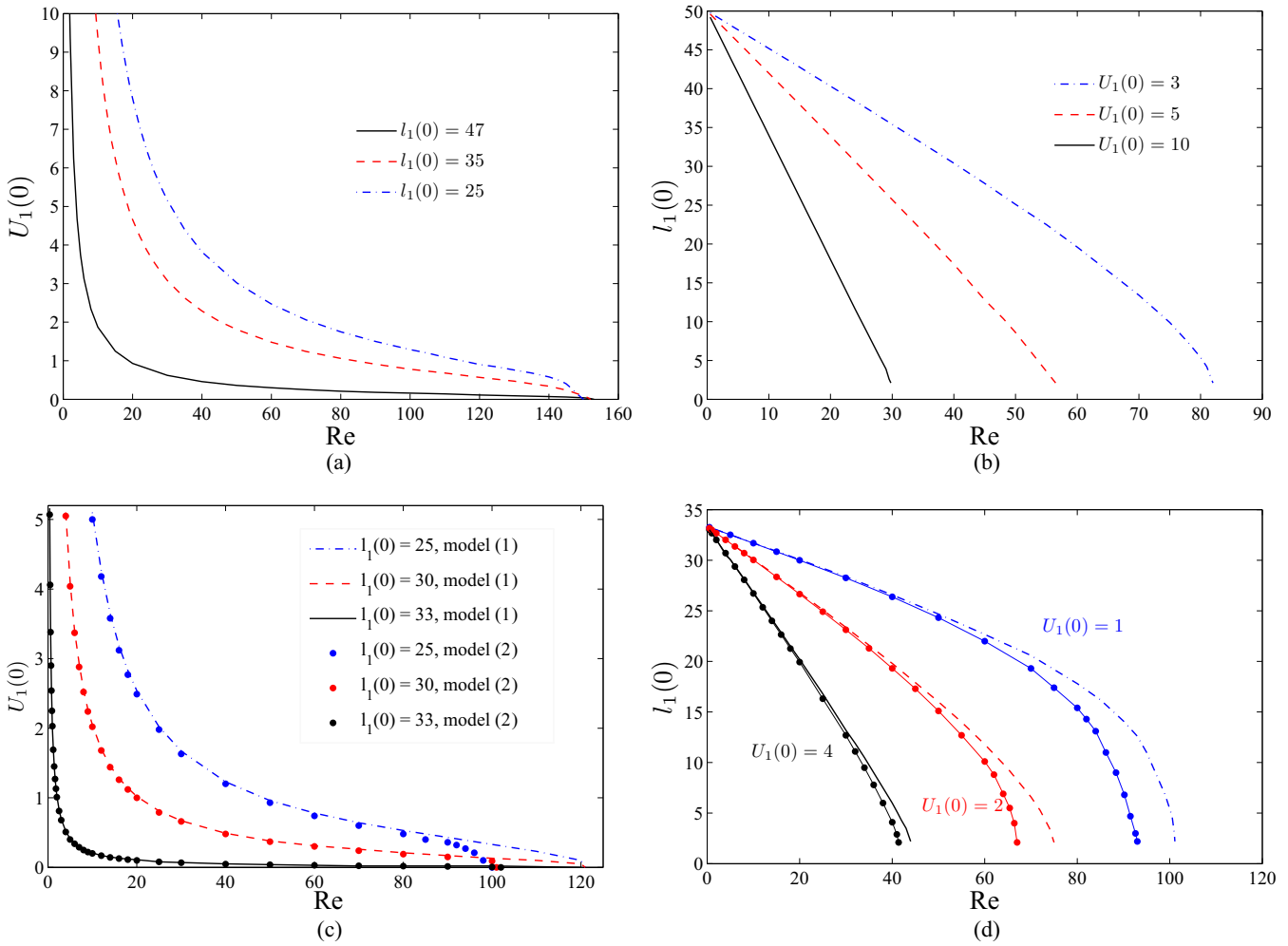

FIG. 7. Domains above the curves in the phase planes correspond to overshooting of initially minimal separation between bubbles l_1. (a,b) two bubbles; (c,d) three bubbles.

do not intersect, $l_1(0) < l/2$ means that l_1 is initially minimal separation, $U_1(0) \sim 10$ correspond to introduction of stationary bubble into the flow, and $U_1(0) > 0$ is considered because we are interested in overshooting of the equilibrium value. Figures 7(a) and 7(b) show cross sections of this domain by the planes $l = 100$, $l_1(0) = \text{const}$ and $l = 100$, $U_1(0) = \text{const}$, respectively, for solutions of (21) that correspond to the two-bubble case. One can see that the overshooting is possible at $\text{Re} < 10$, $U_1(0) < 10$ if $l_1(0) > 35$.

To illustrate the critical behavior of a system with three bubbles, we chose the solutions of (26) and (27) for which the number of governing parameters is reduced. Figures 7(c) and 7(d) show cross sections of this domain by the planes $l = 100$, $l_1(0) = \text{const}$ and $l = 100$, $U_1(0) = \text{const}$, respectively. Marked curves are calculated with the pairwise interaction model (2). Again, one can see that the overshooting is possible at $\text{Re} < 10$. At relatively small Re, the domains of overshooting predicted by the two models of interaction are very close, while for higher Reynolds numbers, model (2) predicts a wider domain.

Examples of the evolution of the separation distance at $\text{Re} = 2$ with and without overshooting are given in Fig. 8. In Fig. 8(a) the initial period of a two-bubble system dynamics for $U(0) = 10$ is presented. When $l_1(0) = 47$ an overshooting takes place (see the dashed curves). However, when the initial separation is a little smaller, $l_1(0) = 46.5$, viscous damping overcomes the inertia and the separation approaches equilibrium monotonically. Similarly in the three-bubble case shown in Fig. 8(c), when $U_1(0) = 5$, overshooting takes place for $l_1(0) = 32$ (see the dashed and dotted curves). When the initial separation is a little smaller, $l_1(0) = 31.5$, viscous damping overcomes the inertia and the separation approaches equilibrium monotonically. This regime is shown by solid and dashed dotted lines. The developed stages of the processes are shown in Figs. 8(b) and 8(d), where approaching the equilibrium value is evident. Solid and dashed lines are calculated with nearest-neighbors interaction model (1), while dashed-dotted and dotted lines present the results obtained in the framework of model (2). One can see that model (2) predicts a little higher overshooting and faster approach to the equilibrium for both regimes.

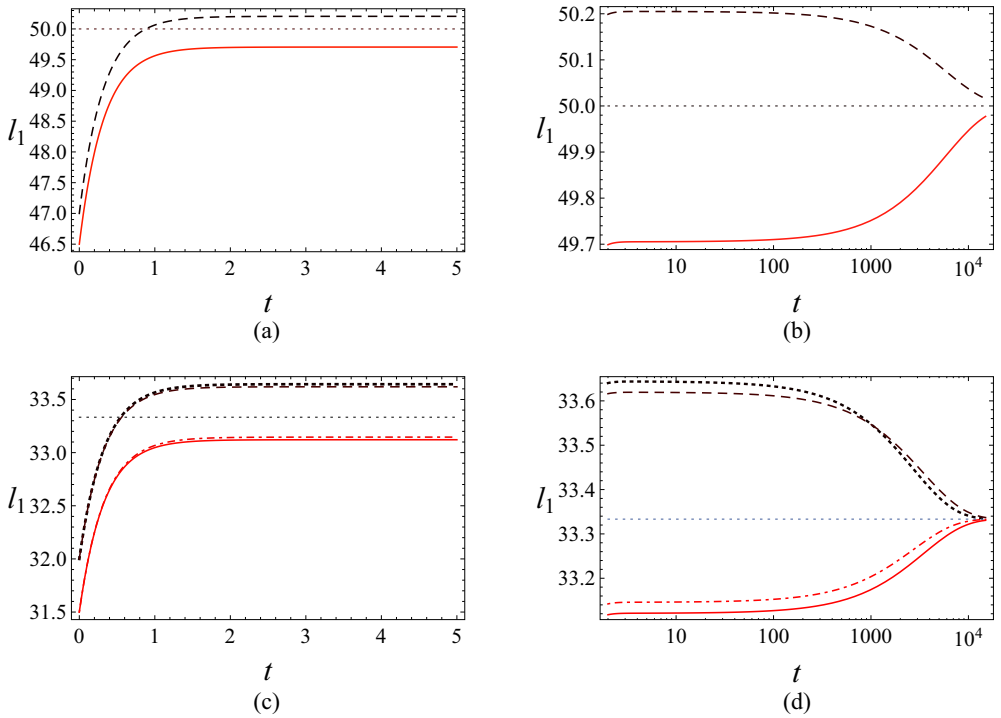

FIG. 8. Evolution of initially minimal separation distance between bubbles. (a) $U(0) = 10$ two-bubble case, initial period $t < 5$; (b) two-bubble case, $U(0) = 10$, long time development $1 < t < 1.5 \times 10^4$; (c) three-bubble case, $U_1(0) = 5$, initial period $t < 5$; (d) three-bubble case, $U_1(0) = 5$, long time development $1 < t < 1.5 \times 10^4$. Solid and dashed lines are calculated with model (1), dashed-dotted and dotted lines are obtained in the framework of model (2).

IV. CONCLUSIONS AND DISCUSSION

In this paper, we studied the effect of added mass on the evolution of separation between interacting bubbles in a Couette-Taylor device. Two simplified models of such dynamics are suggested based on the interaction force found in our previous work [26]. One model assumes that each bubble interacts solely with its nearest neighbors, while the second one takes into account pairwise interactions of all the bubbles in the system. The application of the models results in systems of nonlinear ordinary differential equations describing the evolution of the separations between the bubbles.

The resulting systems of ordinary differential equations were studied first by linearization in the vicinity of the equilibrium. The existence of a critical Reynolds number was reported. Below the critical Reynolds number no oscillations were observed and the relaxation time decreases with an increase in the number of bubbles. Beyond the critical Reynolds number the separations between the bubbles start oscillating until the bubbles reach equilibrium position. The linear theory predicts that the critical Reynolds number grows fast with the ratio of the length of streamline to the bubble radius, and at $l = O(100)$ that is typical for the experiments described in [24–26], $\mathrm{Re}^{\mathrm{cr}} = O(10 - 10^2)$.

Nonlinear effects were studied via numerical integration of governing equations for various initial conditions in the cases of two and three bubbles. It is demonstrated that the critical Reynolds number is lower than that predicted by linearized equations, and remains at $O(10 - 10^2)$. Thus for the experimental conditions, the theory predicts only subcritical regimes. However, in contrast to the theory of [26], where initially the shortest separation distance between the bubbles remained the shortest and approached equilibrium value monotonically from below, the models of the present paper predict overshooting of the equilibrium value for certain initial conditions even for subcritical values of Re, typical for the experiments.

We conclude that the effects taken into account by our model can result in a nonmonotonic behavior of the separation distances between bubbles in a Couette-Taylor flow similar to those observed in several experimental runs reported in [26], that were not explained with the model suggested there. Note that qualitatively similar behavior was predicted by a low-viscosity model of [27] for Reynolds numbers of $O(10 - 10^2)$. Since in the experiments described in [24–26] Re were typically of $O(1)$ the direct comparison of those results with the experiments was not possible. In contrast to this, the model developed in this paper predicts nonmonotonic behavior of separation distance also for experimental values of $\mathrm{Re} \sim O(1)$.

The forces acting on an individual bubble in the system, that are taken into account by the models, are as follows:

The inertia-induced force exerted on a bubble interacting between other bubbles in shear flow. This force is proportional to the Reynolds number and, at the leading order, depends solely on the geometry of the system (the distances between bubbles). Thus it is somewhat analogous to mass forces.

Added mass force induced by the inertia of a volume of fluid that is moved by an accelerating bubble while translating through it. This force depends on the accelerations of the bubbles.

Damping viscous drag that, under low-Re assumption of this paper, is close to the Stokes drag.

The three regimes of bubbles dynamics found in the paper can be related to the relative importance of these forces. When viscous drag dominates, a monotonic approach to the equilibrium takes place. However, for high enough initial relative velocity, the inertia of fluid moved by bubble translation is not damped fast enough and overshooting of equilibrium occurs. If the Stokes drag is low compared to the inertia-induced forces, i.e., at high supercritical Reynolds numbers, oscillations that are typical for the systems without damping are observed.

Note also that both low- and high-viscosity models predict the same order of magnitude for the critical value of the Reynolds number (at the bubble scale) beyond which oscillations are anticipated. These values cannot be achieved at Couette-Taylor devices used in experiments of [24–26] with a stationary outer cylinder. However, for the devices with two rotating cylinders, stable Taylor vortices exist for much higher Re (at the device scale), probably allowing at least values of Re of $O(10)$. It would be interesting to check if supercritical regimes of bubble interaction predicted by the theory can be observed experimentally.

ACKNOWLEDGMENTS

The work was supported by Israel Science Foundation (Grant No. 668/11). O.L. acknowledges the support of the Israel Ministry of Immigrant Absorption. J.P. acknowledges partial support by a fellowship from Israel Council for Higher Education.

[1] P. K. Dutta and A. K. Ray, Experimental investigation of Taylor vortex photocatalytic reactor for water purification, Chem. Eng. Sci. **59**, 5249 (2004).

[2] T. Imamura, K. Saito, S. Ishikura, and M. Nomura, A new approach to continuous emulsion polymerization, Polym. Int. **30**, 203 (1993).

[3] K. Kataoka, N. Ohmura, M. Kouzu, Y. Simamura, and M. Okubo, Emulsion polymerization of styrene in a continuous Taylor vortex flow reactor, Chem. Eng. Sci. **50**, 1409 (1995).

[4] G. Baier, M. D. Graham, and E. N. Lightfoot, Mass transport in a novel two-fluid Taylor vortex extractor, AIChE J. **46**, 2395 (2000).

[5] M. Kim, K. J. Park, K. U. Lee, M. J. Kim, W.-S. Kim, O. J. Kwon, and J. J. Kim, Preparation of black pigment with the Couette–Taylor vortex for electrophoretic displays, Chem. Eng. Sci. **119**, 245 (2014).

[6] J.G. Sczechowski, C.A. Koval, and R.D. Noble, A Taylor vortex reactor for heterogeneous photocatalysis, Chem. Eng. Sci. **50**, 3163 (1995).

[7] B. Haut, H. Ben Amor, L. Coulon, A. Jacquet, and V. Halloin, Hydrodynamics and mass transfer in a Couette–Taylor bioreactor for the culture of animal cells, Chem. Eng. Sci. **58**, 777 (2003).

[8] R. L. Miller, A. G. Fredrickson, A. H. Brown, and H. M. Tsuchiya, Hydromechanical method to increase efficiency of algal photosynthesis, Ind. Eng. Chem. Process Des. Dev. **3**, 134 (1964).

[9] B. Kong, J. V. Shanks, and R. D. Vigil, Enhanced algal growth rate in a Taylor vortex reactor, Biotechnol. Bioeng. **110**, 2140 (2013).

[10] A. Oasmaa, D. C. Elliott, and S. Muller, Quality control in fast pyrolysis bio-oil production and use, Environ. Prog. **28**, 404 (2009).

[11] B. Kong, and R. D. Vigil, Simulation of photosynthetically active radiation distribution in algal photobioreactors using a multidimensional spectral radiation model, Bioresour. Technol. **158**, 141 (2014).

[12] M. Ramezani, B. Kong, X. Gao, M. G. Olsen, and R. D. Vigil, Experimental measurement of oxygen mass transfer and bubble size distribution in an air–water multiphase Taylor–Couette vortex bioreactor, Chem. Eng. J. **279**, 286 (2015).

[13] Y. Murai, H. Oiwa, and Y. Takeda, Frictional drag reduction in bubbly Couette-Taylor flow, Phys. Fluids **20**, 034101 (2008).

[14] T. H. van den Berg, S. Luther, D. P. Lathrop, and D. Lohse, Drag Reduction in Bubbly Taylor-Couette Turbulence, Phys. Rev. Lett. **94**, 044501 (2005).

[15] T. H. van den Berg, D. P. M. van Gils, D. P. Lathrop, and D. Lohse, Bubbly Turbulent Drag Reduction Is a Boundary Layer Effect, Phys. Rev. Lett. **98**, 084501 (2007).

[16] K. Sugiyama, E. Calzavarini, and D. Lohse, Microbubbly drag reduction in Taylor-Couette flow in the wavy vortex regime, J. Fluid Mech. **608**, 21 (2008).

[17] D. P. M. van Gils, D. N. Guzman, C. Suny, and D. Lohse, The importance of bubble deformability for strong drag reduction in bubbly turbulent Taylor-Couette flow, J. Fluid Mech. **722**, 317 (2013).

[18] R. Maryami, S. Farahat, P. M. Javad, and M. M. H. Shafie, Bubbly drag reduction in a vertical Couette-Taylor system with superimposed axial flow, Fluid Dyn. Res. **46**, 055504 (2014).

[19] R. Campero and R. Vigil, Spatiotemporal Patterns in Liquid–Liquid Taylor–Couette–Poiseuille Flow, Phys. Rev. Lett. **79**, 3897 (1997).

[20] R. Campero and R. Vigil, Flow patterns in liquid–liquid Taylor–Couette–Poiseuille flow, Ind. Eng. Chem. Res. **38**, 1094 (1999).

[21] H. Djeridi, C. Gabillet, and J. Y. Billard, Two-phase Couette–Taylor flow: Arrangement of the dispersed phase and effects on the flow structures, Phys. Fluids **16**, 128 (2004).

[22] G. N. Fokoua, C. Gabillet, A. Aubert, and C. Colin, Effect of bubble's arrangement on the viscous torque in bubbly Taylor-Couette flow, Phys. Fluids **27**, 034105 (2015).

[23] R. Maryami, S. Farahat, M. JavadPour, and M. Shafiei Mayam, Frictional drag reduction using small bubbles in a Couette-Taylor flow, J. Mar. Sci. Technol. **20**, 652 (2015).

[24] R. Deng, C.-H. Wang, and K. A. Smith, Bubble behavior in a Taylor vortex, Phys. Rev. E **73**, 036306 (2006).

[25] L. Byk, O. Lavrenteva, R. Spivak, and A. Nir, Interaction and ordering of bubbles levitated in vortical flow, Microgravity Sci. Technol. **19**, 78 (2007).

[26] J. Prakash, O. M. Lavrenteva, L. Byk, and A. Nir, Interaction of equal size bubbles in shear flow, Phys. Rev. E **87**, 043002 (2013).

[27] J. Prakash, O. M. Lavrenteva, and A. Nir, Interaction of equal size bubbles in inviscid and low viscosity shear flow, Phys. Rev. E **88**, 023021 (2013).

[28] J. Happel and H. Brenner, *Low Reynolds Number Hydrodynamics: With Special Applications to Particulate Media* (Kluwer Academic Publishers, Amsterdam, 1983).